JOURNAL OF CHEMICAL PHYSICS VOLUME 118, NUMBER 13 1 APRIL 2003

Density-functional theory studies of xanthate adsorption on the pyrite $FeS_2(110)$ and (111) surfaces

Andrew Hung, Irene Yarovsky, and Salvy P. Russo[a)]
Department of Applied Physics, RMIT University, GPO Box 2476V, Melbourne, Victoria 3001, Australia

(Received 16 October 2002; accepted 7 January 2003)

We have used the density functional theory (DFT) method with a plane wave-pseudopotential basis to compute the structure and properties of a model xanthate molecule ($HOCS_2^-$) and its adsorption characteristics on the pyrite $FeS_2(110)$ and (111) surfaces. Molecular calculations revealed that $HOCS_2^-$ and $CH_3CH_2OCS_2^-$ have similar head group electronic structure and, therefore, the use of the model xanthate is a justifiable approximation in simulations of xanthate head group attachment to FeS_2 surfaces. Results from DFT calculations suggest that $HOCS_2^-$ readily undergoes dissociation at the fourfold coordinated surface Fe on the (110) surface, and the bridging S of the (111) surface. These results suggest that xanthate may undergo chemisorption at defect sites on real FeS_2 surfaces, which contain low-coordinate Fe sites and sites in proximity to cleaved S–S bonds. © *2003 American Institute of Physics.* [DOI: 10.1063/1.1556076]

I. INTRODUCTION

Froth flotation is an important technique for the separation and concentration of valuable transition metal sulphide minerals such as sphalerite and chalcopyrite from the crude ore.[1] In this process, collector molecules are often added to the flotation pulp in order to enhance the hydrophobicity of the desired ores. This is facilitated through the binding of the head group of the molecules to the particle surfaces and subsequent coverage of the surfaces with their hydrophobic "tails." Pyrite (FeS_2) is often present together with valuable sulphide ores, and constitutes an undesirable presence when valuable minerals are to be separated from their ores by froth flotation, largely due to extensive deposition of collector molecules on its surface, leading to its flotation and subsequent contamination of the desired mineral.[2] It would therefore be more economical to use collectors that bind effectively to the desired sulphide mineral, while having little or no affinity for FeS_2 surfaces. One of the most commonly used flotation collectors in sulphide mineral extraction are the alkyl xanthates, which are known from early flotation practice to deposit on pyrite surfaces.[3] Thus, in order to design more efficient flotation collectors for future applications, it is important to develop an understanding of the interaction between the xanthate head group and FeS_2 surfaces at the molecular level, and in particular to determine the primary cause of their mutual affinity.

Several mechanisms for the adsorption of xanthate on FeS_2 surfaces have been proposed based on experimental evidence. The xanthate ion itself has been identified as the most stable species under alkaline conditions ($p\mathrm{H}>11$) in several early studies using various spectroscopic, electrokinetic, and electrochemical techniques,[4–7] and therefore under such conditions, may be the species responsible for adsorption to FeS_2. Other species have also been determined to contribute to FeS_2 flotation, including the xanthate dimer dixanthogen,[8] various metal complex species,[9] as well as metal hydroxide complexes.[10] Further examples of collector-induced flotation of pyrite and other sulphide minerals may be found in a review article by Persson.[11]

There is some evidence which suggests that the xanthate ion undergoes chemisorption on FeS_2 surfaces in an oxygen-free environment.[12] Previous *ab initio* calculations of xanthate surface interaction,[13] though, suggest that the ion does not readily adsorb to the (100) surface. However, in the study mentioned above, the surface was modelled as a defect-free terrace, although real (100) FeS_2 surfaces are known to have poor cleavage, which result in high surface defect density. Thus, despite the results presented in Ref. 13, it is possible that xanthate ions may undergo chemical reaction at defect sites on real surfaces, a small number of which may persist (i.e., remain unoxidized) under conditions of low O_2 concentration. Studies of the effects of surface imperfections on CH_3OH and H_2O adsorption[14] revealed the persistence of oxygen at defect sites even after temperature-programmed desorption, which suggests some dissociation at these sites. Under certain conditions, then, it is possible that xanthate ions may also undergo dissociation at defect sites. In the present work, we focus on simulating the interaction between xanthate ion and pyrite surface defects, which are modelled using the nondipolar (110) and (111) surfaces, as discussed below.

Despite the wealth of information that have been collected from experimental studies, the precise mechanism responsible for surface hydrophobation is still a contentious issue, and discrepancies exist in the literature due to the difficulties of studying interfaces *in situ*. Such difficulties may in principle be overcome by the use of computer simulation which, in addition to illuminating the fundamental aspects of adsorption, can also aid in the interpretation of experimental results. The increased sophistication of *ab initio* quantum chemical methods, coupled with a growth in computer

---

[a)] Author to whom correspondence should be addressed. Tel.: +61(3)9925 2601; Fax: +61(3)9925 5290; electronic mail: salvy.russo@rmit.edu.au

0021-9606/2003/118(13)/6022/8/$20.00

power, means that it is now possible to model complex physical and chemical systems. Simulation is therefore becoming established as a complementary technique to experiment for the study of mineral surfaces, as it can provide valuable primary information on well-characterized systems and allows for structural, chemical, and stoichiometric effects to be isolated. Recent work has demonstrated that *ab initio* techniques, and in particular, those based on density-functional theory (DFT), can provide remarkable insights into the structure and properties of FeS_2 surfaces,[15] as well as their oxidation mechanisms.[16] Moreover, our previous work on the application of DFT methods to the study of FeS_2 surfaces[17,18] has provided a foundation for the current investigation of xanthate adsorption.

There are at present very few published computational studies of collector adsorption on mineral surfaces, and to date, there are no published reports of *ab initio* simulations of the xanthate–pyrite interaction. However, the adsorption of 2-mercaptobenzothiazole (MBT) ion (a commonly-used flotation collector) and MBT dimer onto the FeS_2 surface has been studied using semiempirical extended-Huckel cluster calculations.[19] It was found that both species chemically bind to surface Fe without dissociation, but the dimer was found to adsorb more strongly. Molecular DFT calculations of the structure and properties of xanthate, dixanthogen and various metal-xanthate complexes have been reported by Tossell *et al.*[20] (some of the results acquired from the latter study are discussed and compared with our findings in Sec. III). In addition, we have performed plane wave-pseudopotential DFT simulations of xanthate and xanthate–iron–hydroxide complex adsorption on the (100) surface.[13] These calculations indicated that while the xanthate ion itself does not readily adsorb to the (100) surface, but binding of a xanthate–iron–hydroxide complex was found to be energetically favorable.

In the present work, we apply the density-functional theory (DFT) method using a plane wave-pseudopotential basis set to model the adsorption of the xanthate ion head group ($-OCS_2-$) onto the (110) and (111) surfaces of pyrite. Since the nondipolar, highly reactive $FeS_2(110)$ and (111) surfaces are terminated by defectlike species such as undercoordinated Fe and severed S–S bonds (prevalent on real pyrite surfaces, which cleave conchoidally), simulation of xanthate adsorption on these highly reactive surfaces may yield insights into xanthate reactions at defect sites on real pyrite surfaces. A model xanthate, $HOCS_2^-$, was used in place of ethyl xanthate in order to allow efficient computation while sacrificing little in terms of head group property calculation, as discussed in Sec. III.

II. COMPUTATIONAL DETAILS

Geometry optimization of bulk FeS_2 and all surface relaxation calculations were performed within the framework of DFT, using a generalized gradient spin approximation (GGSA) (Ref. 21) Perdew–Wang exchange-correlation functional[22] and a plane wave-pseudopotential basis as implemented in the Vienna *Ab Initio* Software Package (VASP) code.[23–25] Ultrasoft pseudopotentials[26] for Fe and S as supplied in the VASP package were used in this study. A plane wave cutoff energy of 396 eV was used for all calculations. **k**-space sampling was performed using the Monkhorst–Pack scheme.[27] Previous studies on (1×1) FeS_2 surfaces[17,18] have revealed that the surface energies and atomic displacements due to structural relaxations are converged to within the prescribed tolerance levels of 0.001 J/m^2 and 0.001 Å, respectively, using a 4×4×1 **k**-point mesh. In the present work, adsorption studies were performed using surface supercells corresponding to (2×2) surface unit cells, as discussed below. Subsequently, 2×2×1 **k**-point sampling meshes were used for all adsorption calculations.

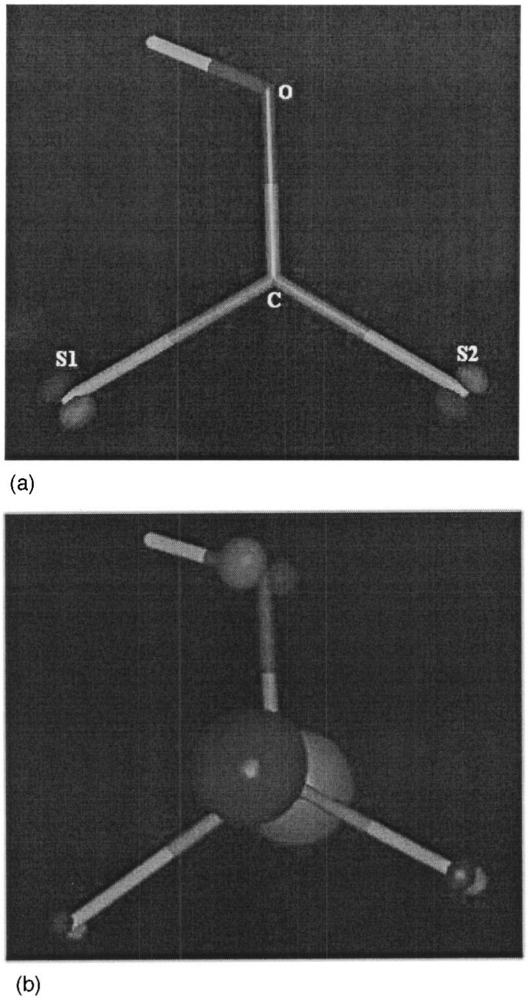

FIG. 1. (a) Hydrogen xanthate HOMO isosurface (DMOL PWGGA). (b) Hydrogen xanthate LUMO isosurface (DMOL PWGGA).

The minimum-energy geometry and electronic structure of the model xanthate molecule ($HOCS_2^{2-}$) was computed using the DMOL (Ref. 28) code, which employs numerical basis functions expressed as values on an atomic-centered spherical-polar mesh. The use of DMOL in computing the electronic structure of the molecular species allows convenient qualitative comparison of the frontier orbital topologies of the various xanthates, which were visualized using the Insight II (Ref. 29) software suite [Figs. 1(a) and 1(b)]. This is important in establishing the validity of using $HOCS_2^-$ as a model for alkyl xanthates in subsequent adsorption calculations. DMOL calculations were performed using the PWGGA functional and the double-zeta (DZ) all-electron basis set with polarization functions on all atoms. Geometry optimization calculations were performed using an eigenvector-following (EF) algorithm[30] using BFGS Hessian update, with gradient, atomic displacement and energy convergence tolerances of 0.001 eV/Å, 0.001 Å, and 0.00001 eV, respectively.

All adsorbate–surface systems were modelled using the supercell approach in VASP. The surfaces were obtained from the relaxed bulk structure acquired using the PWGGA functional, with the computed lattice parameter (a_0) of 5.431 Å and internal coordinate (x_s) of 0.383 (Ref. 17). The initial geometry of the xanthate ion in the adsorption calculations was taken as the computed minimum-energy structure acquired from PWGGA structure relaxation calculation using VASP (see Sec. III), with the xanthate ion inside a 20×20×20 Å supercell. In order to minimize spurious mirror-image interactions between xanthate molecules in adjacent supercells, surface adsorption was modelled by placing single xanthate molecules in the vicinity of (2×2) surfaces, corresponding to coverages of one molecule per 166.85 and 204.35 Å^2 for the (110) and (111) surfaces, respectively. In addition, in order to avoid interactions between the xanthate adsorbate and the mirror image surface, vacuum separations of 10 Å were placed between the topmost atom (belonging to the xanthate moiety) and the outermost atoms of the surface slab in the adjacent mirror image supercell parallel to the surface plane. Full geometry optimizations were performed for all adsorption systems studied using the conjugate-gradient algorithm implemented in VASP. Geometric constraints were placed on the central atomic layer of the surface slabs in order to avoid drift during the course of optimization.

As discussed in Refs. 17 and 18, 12 atomic layer-thick slabs were required for modelling the (110) surface in order to obtain computed surface energies converged to within 0.01 J/m^2, while a 15 atomic-layer thick slab was required for the (111) surface to reach a similar degree of numerical accuracy. However, due to the computational expense involved in simulations of surface adsorption using supercells corresponding to (2×2) surface unit cells, in the current work, slab thicknesses corresponding to three (3) surface unit cells were used for adsorption on the (110) surface (i.e., 9 atomic layers), and two (2) surface unit cells for adsorption on the (111) surface (10 atomic layers). It was found that the choice of these slab thicknesses resulted in negligible relaxation near the centers of the slab, as discussed in Sec. IV.

III. XANTHATE STRUCTURE AND PROPERTIES

In the current study, the interaction between the xanthate head group and FeS$_2$ surfaces were studied using a model xanthate, HOCS$_2^-$, although ethyl xanthate CH$_3$CH$_2$OCS$_2^-$ is commonly used in experimental studies. In using such a model, it is assumed that the hydrophobic ethyl group has little influence on the properties of the head group, and therefore does not affect physical or chemical interactions between the head group and FeS$_2$ surfaces. In order to determine the validity of this assumption, we have compared the computed minimum energy geometries, atomic Mulliken populations,[31] and highest-occupied molecular orbital (HOMO) and lowest-unoccupied molecular orbital (LUMO) topologies of methyl, ethyl, and hydrogen xanthate molecules (corresponding to CH$_3$CH$_2$-, CH$_3$-, and H–OCS$_2^-$, respectively) using the molecular *ab initio* software DMOL.

Atomic labels for the OCS$_2$ head group are indicated in Fig. 1(a), and are referred to as such in all subsequent discussions of xanthate properties and surface adsorption in the remainder of this paper. Bond distances and angles for the ethyl, methyl, and hydrogen xanthate species at their minimum energy geometries are given in Table I, indicating the similarity in head group geometry of these species. The Mulliken charges for the head groups of the xanthate species are given in Table II. We note that, although it is not possible to unambiguously assign charges to particular atoms in a molecule, Mulliken population analysis may nonetheless be useful as a semiquantitative indication of the relative magnitude of electron density at various atomic sites. In the current work, such information is useful in determining the atomic sites that dominate electrostatic interactions. For all of the xanthate species studied, population analysis indicates that the excess −1 charge is concentrated on, and approximately evenly distributed amongst the two head group sulphur atoms. Furthermore, the charge values for the S1–C–S2 group for both of the alkyl xanthates as well as the hydrogen xanthate are remarkably similar. There is also a negative charge associated with the oxygen site. It is interesting to note that, although the O charge is comparable to that of the two S atoms for HOCS$_2^-$, it is significantly less negative for the alkyl xanthates, indicating that for xanthates with a hydrocarbon chain, electrostatic interactions are likely to occur primarily at the charged S sites. These results also give an indication that the electronic structure of the S1–C–S2 group between the xanthates presently studied are similar in nature,

TABLE I. Methyl, ethyl, and hydrogen xanthate head group bond angles and distances, computed using DMOL, PWGGA functional unless otherwise noted.

	Met-OCS$_2^-$	Et-OCS$_2^-$	HOCS$_2^-$
R (C–O) (Å)	1.43	1.41 (1.35)[a]	1.42 (1.38)[b]
R (C–S1) (Å)	1.71	1.70 (1.67)[a]	1.71 (1.65)[b]
R (C–S2) (Å)	1.72	1.71 (1.70)[a]	1.74 (1.72)[b]
S1–C–S2 bond angle	129°	128.3° (124°)[a]	130° (130°)[b]

[a] Values in brackets indicate experimental values from Ref. 32.

[b] Values in brackets acquired using the PWGGA functional in VASP, taken from Ref. 13.

TABLE II. Methyl, ethyl, and hydrogen xanthate head group Mulliken populations, DMOL.

	Met-OCS$_2^-$	Et-OCS$_2^-$	HOCS$_2^-$
O	−0.35	−0.35	−0.57
C	+0.31	+0.32	+0.29
S1	−0.54	−0.55	−0.54
S2	−0.56	−0.56	−0.57

TABLE III. Hydrogen xanthate head group geometry, xanthate ion with charges −3, −2, 0, +1, DMOL.

	$HOCS_2^{3-}$	$HOCS_2^{2-}$	$HOCS_2$	$HOCS_2^+$
R (C–O) (Å)	1.42	1.40	1.36	1.31
R (C–S1) (Å)	1.90	1.78	1.69	1.73
R (C–S2) (Å)	1.90	1.78	1.70	1.72
S1–C–S2 bond angle	120°	127°	115°	108°

which is further supported by inspection of their frontier molecular orbital structures, as discussed below.

The computed HOMO and LUMO orbitals of $HOCS_2^-$ are shown in Figs. 1(a) and 1(b), respectively. The topologies of these orbitals are very similar for all of the xanthate species studied, with the HOMO dominated by the head group sulphur 3*p* orbital, while the head group carbon 2*p* orbital make the most significant contribution to the LUMO. All of the frontier orbital contributions are thus mainly concentrated at the S1–C–S2 site, and are qualitatively similar across all three molecules. In addition, the topologies of the HOMO and LUMO orbitals give an indication of the dominant sites of chemical interaction of the xanthate head group; namely, that electron donation to the xanthate moiety (corresponding to additional electrons placed in the LUMO) will likely occur at the carbon site, while electron donation from the xanthate (electrons removed from the HOMO) will likely occur through the sulphur sites.

These results indicate the similarity in the head group electronic structure between ethyl and hydrogen xanthate. Since the interaction of interest in the current work is that between the head group and the FeS_2 surfaces, the results discussed above suggest that the use of the model xanthate $HOCS_2^-$, in place of the more realistic $EtOCS_2^-$, is a justifiable approximation. However, we note that the structure of the hydrophobic alkyl group may need to be taken into account in other simulations of flotation, for example, if properties such as surface hydrophobicity modifications are desired. In the present case, however, we are solely interested in the nature and extent of bonding between the head group and the FeS_2 surfaces, in which case the structure of the chain may be neglected.

We have examined the effects of oxidation (electron loss) and reduction (electron gain) on the structure of xanthate by geometry optimization of the $HOCS_2^+$, $HOCS_2$, $HOCS_2^{2-}$, and $HOCS_2^{3-}$ species. The minimum-energy bond lengths and angles of the oxidized ($HOCS_2^+$ and $HOCS_2$) and the reduced ($HOCS_2^{2-}$ and $HOCS_2^{3-}$) species are given in Table III. Comparison of these structures with the optimized structure of $HOCS_2^-$ (given in Table I) shows that oxidation results in no significant change of C–S bond lengths, and a strengthening of the C–O bond, evident in the lowering of the C–O bond length from 1.42 Å in $HOCS_2^-$ to 1.31 Å in $HOCS_2^+$. However, reduction weakens the C–S bonds, enhancing the C–S bond lengths from 1.71 and 1.74 Å in $HOCS_2^-$ to 1.90 Å in $HOCS_2^{3-}$. These results are in agreement with those of Ref. 20, where the Hartree–Fock method was applied for geometry optimizations.

The minimum-energy geometry of $HOCS_2^-$ was also computed using VASP within the PWGGA and the supercell approach. A cubic supercell of dimension 20×20×20 $Å^3$ was used to contain the molecule, corresponding to approximately 15 Å of vacuum separation between adjacent mirror images of the molecule in all three supercell directions. Computed bond lengths and angles for the OCS_2 head group are given in Table I. Comparison between the values acquired using both VASP and DMOL reveal similar predicted head group structure, although a higher C–S bond length difference between the two C–S bonds was predicted using VASP. Differences in basis set, and in particular the nature of the pseudopotential used in VASP may be partially responsible for this disparity.

IV. $HOCS_2^-$ ON THE (110) AND (111) SURFACES

In order to determine the preferred sites of interaction on the FeS_2 surfaces, it is instructive to consider the electrostatic attraction and chemical reactivities of the various surface sites towards adsorbates. We note that, although other nonbonded interactions (due to dispersion forces) may play a role in determining xanthate adsorption (or otherwise), they are negligible in magnitude compared to electrostatic forces, due to the ionic nature of the xanthate head group and the FeS_2 surfaces.

As discussed in Sec. III, the excess electronic charge on the xanthate ion is concentrated on and distributed between the two sulphur sites, while for the (110) and (111) surfaces, the surface Fe species are positively charged, with computed Mulliken charges of approximately +1.2 (Refs. 17 and 18). Electrostatic attraction will therefore be present primarily between the xanthate S sites and at undercoordinated Fe^{2+} sites for all of the surfaces studied. For the (110) surface, the surface DOS indicates that both valence and conduction bands are dominated by surface Fe states,[17] which suggests that both electron donor and acceptor adsorbates will preferentially interact at surface Fe sites for orbital-controlled reactions. Thus, for the (110) surface, regardless of whether the interaction is electrostatic (without charge transfer) or chemical (with possible charge transfer and bond breakage or formation), xanthate will preferentially adsorb at the undercoordinated surface Fe sites. Xanthate interaction at the Fe sites of the (110) surface are discussed below.

For the (110) surface, the plane of the xanthate ion is initially placed perpendicular to the surface, with the xanthate S sites directed towards the surface fourfold coordinated Fe and surface Fe–xanthate S separations of 2 Å. The final minimum-energy configuration is given in Fig. 2(a), which shows an apparent severing of the xanthate C–S1 bond and bond formation between the xanthate C and the surface Fe1. The displaced xanthate S1 forms new bonds with the neighboring Fe2 and a surface S, effectively forming a S_2 dimer bonded to the surface Fe, while S2 is bonded to both Fe2 and the xanthate C. The coordinations around both Fe1 and Fe2 are subsequently increased from 4 (for the clean surface) to 5. Although the highly reactive displaced xanthate S atom was shown to bind to adjacent sites on the (110) surface in the present calculation, it is possible that

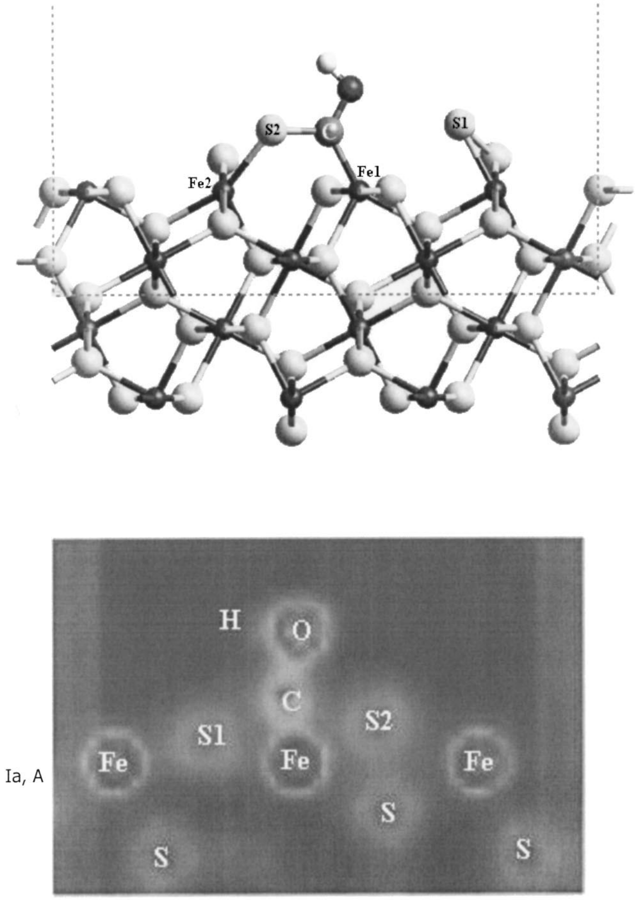

FIG. 2. (a) $HOCS_2^-$ on the $FeS_2(110)$ surface; optimized geometry. (b) Electron density map for $HOCS_2^-$ dissociated on the (110) surface.

such a species would react with H_2O and O_2 present in real solutions to form sulphate species.

Insight into the nature of the bonding between the dissociated xanthate species and the surface Fe sites may be obtained by examining the electron density map plotted along a plane that coincides with the Fe–C bond axis [Fig. 2(b)]. The sulphur atoms corresponding to the dissociated xanthate are labeled S1 and S2, while those of the (110) surface are labeled as S. The enhanced electron density in the Fe–C interatomic region indicates significant covalent character of this interaction. By contrast, the Fe–S interatomic regions below the surface are relatively devoid of electron density, indicating the ionic nature of Fe–S bonding in bulk FeS_2.

By considering the results discussed above and the optimized geometries of both oxidized and reduced $HOCS_2^-$ described in Sec. III, a mechanism for xanthate dissociation may be proposed. It was shown that reduction, corresponding to electron input into the LUMO of xanthate ion, results in weakening of the C–S bond, while oxidation results in no change in C–S bonding but resulted in compression of the C–O bond length. For xanthate dissociation on the (110) surface, there is relatively little change in C–O bond length between the initial and final structures (1.38 Å and 1.34 Å, respectively), suggesting that xanthate is not oxidized. However, the severing of one of the C–S bonds indicates that these bonds are weakened as a result of interaction with the (110) surface, which suggests reduction of the xanthate. Thus, a possible dissociation mechanism is that electron density is transferred from surface Fe to xanthate ion, weakening the C–S bonds and resulting in the cleavage of one, with subsequent Fe–C surface covalent bond formation. The other xanthate C–S bond remains intact, being stabilized by bonding to Fe2. Electron transfer from the surface is likely to be directed at the C site, since the xanthate LUMO is composed mainly of C $2p$ states.

Adsorption of xanthate does not significantly alter surface relaxation in areas that are not near the adsorption site. However, the surface Fe1, which is directly bonded with the dissociated xanthate, undergo less relaxation than the surface Fe sites of the clean surface. On the clean surface, structural relaxations occur primarily to enhance effective Fe coordination.[17,18] However, because bonding with xanthate enhances the coordination around the surface Fe, there is less energetic imperative for geometric relaxation, and the S–Fe–S axis remains approximately 180°. There is negligible atomic displacement below 3 atomic layers.

For the (111) surface, the surface DOS indicates that the upper part of the valence band has a significant contribution from the surface bridging S, while the conduction band is dominated by the surface sixfold coordinated Fe bonded to the bridging S, with some contribution from the neighboring fivefold coordinated Fe site. This suggests that electron donation from the surface to the adsorbate will take place preferentially at the bridging S, while electronic charge transfer to the surface will occur at the sixfold Fe site. However, due to its high coordination number, access to the sixfold Fe site will be restricted, and it is therefore more likely that electron acceptance will take place at the neighboring fivefold coordinated Fe site. Therefore, for the (111) surface, several adsorption geometries are possible. First, xanthate may interact electrostatically with the surface fivefold Fe site as mentioned above; as an electron donor at the same site; or as an electron acceptor at the bridging S site. We discuss the interactions at these two sites below.

In the first initial adsorption geometry for xanthate on the (111) surface, the xanthate C and S sites are directed towards the surface bridging S, whose states dominate in the upper part of the valence band of the surface DOS. The xanthate S and surface S separation is initially 2 Å. The final geometry is as shown in Fig. 3(a), indicating dissociation of the xanthate ion through cleavage of a single C–S bond (originally between C and S2 labeled in the figure), in direct analogy with the results obtained for the (110) surface. In this case, electron transfer occurs from the surface S to xanthate, concentrated mainly on the C site. This results in covalent bond formation between C and the bridging S3, as suggested by the electron density map passing through the bond axis [Fig. 3(c)].

A top view of the optimized structure is shown in Fig. 3(b). In Ref. 18, it was noted that surface bridging S atoms relax laterally, probably due to electrostatic attraction to neighboring surface fivefold coordinated Fe sites. For the clean surface, such sites undergo absolute displacements of approximately 0.4 Å. In the present case, it was found that

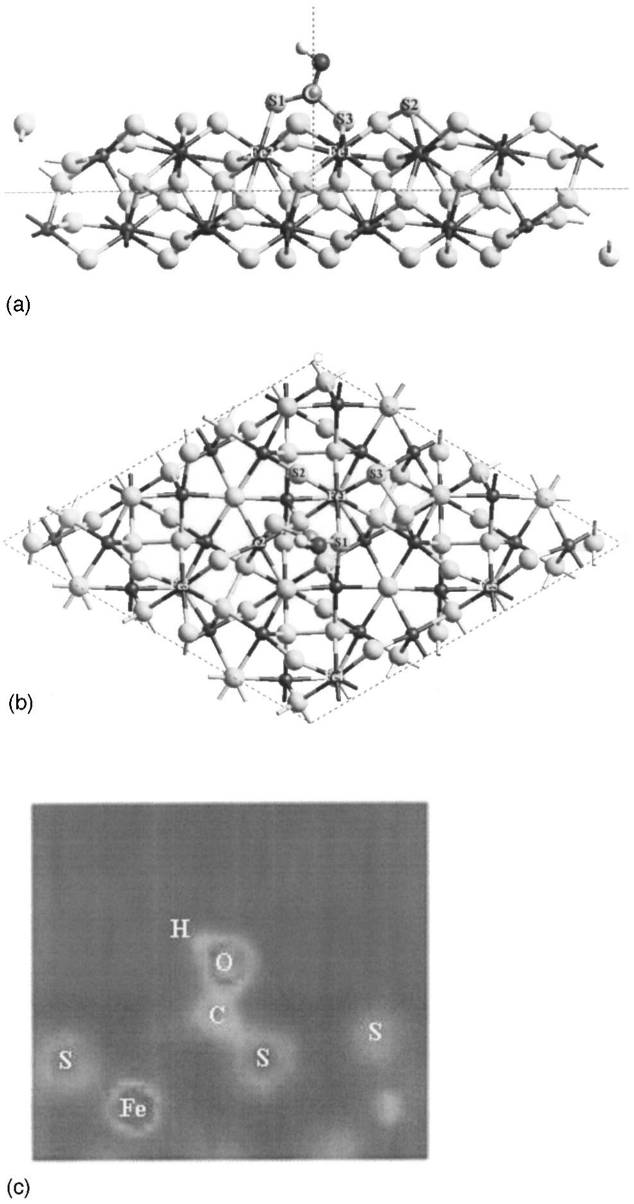

FIG. 3. (a) $HOCS_2^-$ on the $FeS_2(111)$ surface; optimized geometry. (b) $HOCS_2^-$ on the $FeS_2(111)$ surface; optimized geometry, top view. (c) Electron density map for X-dissociated on the (111) surface.

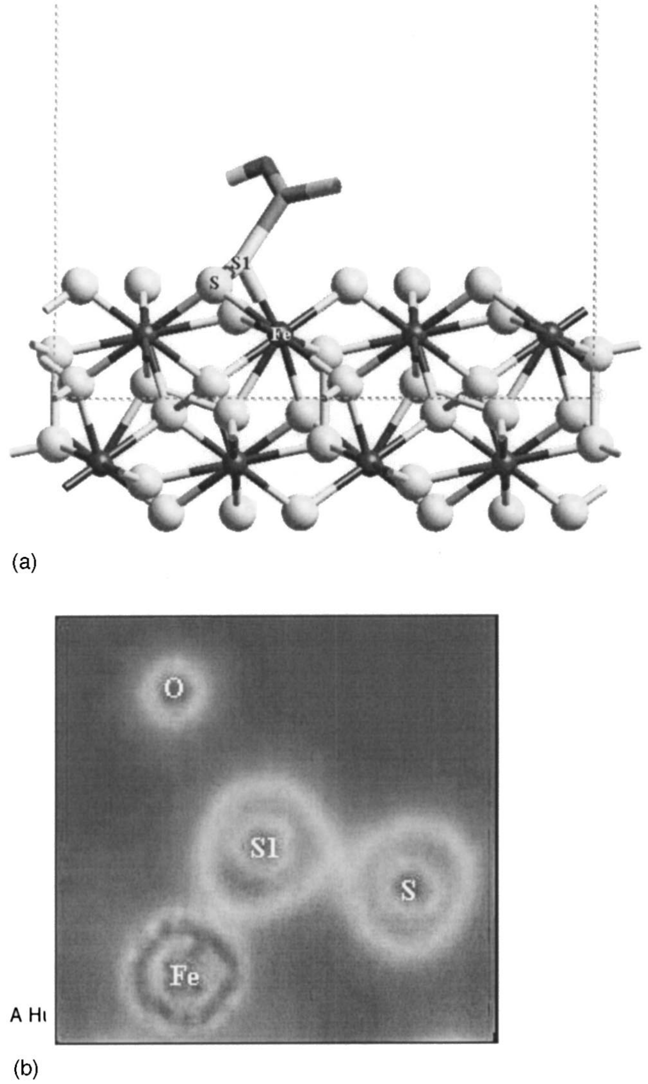

FIG. 4. (a) $HOCS_2^-$ on the $FeS_2(111)$ surface; final geometry. (b) Electron density map for X, doubly bonded on the (111) surface.

the S site directly bonded to the dissociated xanthate species (labeled S1, bonded to Fe1) undergoes an absolute displacement of 0.07 Å, much less than that for the clean surface. This is likely to be due to reduction in translational freedom as a result of covalent bonding with the dissociated xanthate. In addition, bridging S atoms in proximity to the adsorption site are also affected [labeled S2 and S3, bonded to Fe1 in Fig. 3(b)]. These displace by 0.1 and 0.07 Å, respectively. The reason for the reduction in displacements of S2 and S3 may be due to lowered electrostatic attraction between S2 and the (originally) fivefold coordinated surface Fe2 site, which is complexed to the adsorbed xanthate. In the present calculations, S3 is bonded to the S atom dissociated from the original xanthate ion, and thus undergo low atomic displacement. Bridging S further away from the adsorption site (bonded to Fe3, Fe4, and Fe5) displace by approximately 0.20 Å each, roughly half of that computed for the clean surface. Similarly to the (110) surface, atomic displacements are minimal below 3 atomic layers.

In the second initial adsorption geometry for xanthate on the (111) surface, the xanthate C and S sites are placed in proximity to the surface fivefold coordinated Fe, whose states dominate in the lower part of the conduction band of the surface DOS. The xanthate S and surface Fe are initially at 2 Å separation. The optimized geometry is shown in Fig. 4(a). The xanthate ion apparently remains intact, with one sulphur (labeled S1) coordinated to a nearby bridging S (labeled S) as well as an adjacent fivefold coordinated Fe (labeled Fe) with interatomic separations of 2.20 and 2.14 Å, respectively. The C–S1 bond is 1.94 Å, which is elongated relative to the free $HOCS_2^-$ C–S bond lengths of 1.71 and 1.68 Å. The weakening of the C–S1 bond is indicative of electron transfer from the surface to the ion, as discussed in Sec. III. However, unlike the cases of adsorption at the (110) surface and the S site of the (111) surface, the structural relaxation calculation for this system did not predict dissociation of the xanthate. This indicates a lesser degree of C–S bond weakening compared to the previous two cases. Consequently, this also suggests a lower amount of net electron density transfer to the xanthate ion. The adsorbate–surface bonding may be rationalized by considering the contributions of the two surface species to the surface DOS in the valence region. It may be postulated that electron density is transferred to the xanthate ion from the surface bridging S (which dominates the upper part of the valence band), resulting in weakening of the C–S1 bond. We note that, although the xanthate LUMO is composed primarily of C 2*p* character, there is some contribution from the S *p* states, and thus the adsorbate may well accept electrons from the surface at the S sites. However, a lesser amount of electron density is also transferred from the S1 site to the fivefold surface Fe (which dominates the lower part of the conduction band), and as a result, reduces the net amount of electron addition to the xanthate, stabilizing the ion against bond breakage. Since, according to the above description, there is greater electron transfer between S1 and S than between S1 and Fe, it is postulated that there is a greater degree of interaction for the former compared with the latter. The nature of both bonds is illustrated in the electron density map that coincides with the Fe–S1–S plane [see Fig. 4(b)]. Both bonds appear to have mixed character, with the S–S1 interaction apparently more covalent, having greater electron density in the interatomic region.

The results discussed above suggest that xanthate may dissociate and subsequently chemisorb at exposed defect sites such as steps and cleaved S–S bonds on real pyrite surfaces, provided that some of these sites remain unoxidized. This may be possible for pyrite surfaces in oxygen-free environments. However, in the presence of H_2O and O_2, such defect species on real pyrite surfaces are likely to be highly reactive, and would rapidly oxidize, passivating them against further reaction with xanthate. Thus, dissociation at unoxidized defect sites is not likely to be the primary mechanism responsible for collector-induced flotation in oxygen-rich environments, although it may still contribute to the process to a small extent.

V. CONCLUSIONS

We have used the DFT method with a plane wave-pseudopotential basis to compute the structure and properties of a model xanthate molecule ($HOCS_2^-$) and its adsorption characteristics on the FeS_2(110) and (111) surfaces. Calculations show that the electronic structure of the head group are very similar for hydrogen, methyl and ethyl xanthate ions, and confirmed the validity of using the hydrogen xanthate in simulations of head group interaction with FeS_2 surfaces. Results from DFT calculations suggest that $HOCS_2^-$ is likely to dissociate at the fourfold coordinated surface Fe on the (110) surface, and the bridging S of the (111) surface. $HOCS_2^-$ was also found to bind to the fivefold Fe site on the (111) surface. These results suggest that xanthate may undergo chemisorption at low-coordinated Fe sites and sites in proximity to cleaved S–S bonds on real FeS_2 surfaces. This is in contrast to the behavior of xanthate in proximity to the clean (100) surface as determined using plane wave-pseudopotential simulations, where the ion was found to be repelled at the surface.[13] The results reported in the present work is in qualitative agreement with published experimental findings which suggest that, in oxygen-free environments where some defect sites may remain unoxidized, the xanthate ion may undergo chemisorption at the FeS_2 surface.

In order to fully understand the factors involved in collector-induced flotation of FeS_2, and ultimately in designing collectors which allows selective flotation of valuable sulphide minerals while preventing flotation of gangue minerals like FeS_2, it is necessary to examine other mechanisms that may be responsible for collector-induced hydrophobation. However, as noted previously in this and other works, there are numerous possible mechanisms for FeS_2 flotation. The current work may therefore be extended in many possible directions. Further work on the xanthate–FeS_2 system may include studies of the surface adsorption of other xanthate complexes, some of which may be high in concentration under various solution conditions. Dixanthogen has been implicated as one of the major species responsible for FeS_2 flotation, and it would be beneficial to gain a more complete understanding of its formation mechanism and adsorption characteristics. Additionally, the nature of the surface itself needs to be taken into account. For example, real FeS_2 surfaces exposed to air and water will likely be covered with oxidation species, and more realistic simulations will therefore involve investigations of collector (and collector-derived species) adsorption onto such surfaces. Generally, then, future directions in the use of computational simulation in this area of research will likely focus on the design of collectors which do not themselves attach to clean or oxidized FeS_2 surfaces, nor form derivatives (such as dimers and hydroxide complexes) which have a high propensity for doing so.

ACKNOWLEDGMENTS

The authors thank Dr. Joseph Muscat (Daresbury Laboratories, U.K.) for helpful discussions and advice on the current work. Provision of computer resources by the Victorian Partnership for Advanced Computing (VPAC) and the Australian Partnership for Advanced Computing (APAC) is gratefully acknowledged.

[1] K. L. Sutherland and I. W. Wark, *Principles of Flotation* (Australian Institute of Mining and Metallurgy Inc., Melbourne, Australia, 1955).

[2] *SME Mineral Processing Handbook*, edited by N. Weiss (Society of Mining Engineers, New York, 1985).

[3] A. M. Gaudin, F. Dewey, W. E. Duncan, R. A. Johnson, and O. F. Tangel, Trans. AIME **112**, 319 (1934).

[4] M. C. Fuerstenau, M. C. Kuhn, and D. A. Eligillani, Trans. AIME **205**, 65 (1956).

[5] H. Majima and M. Takeda, Trans. AIME **241**, 431 (1968).

[6] A. H. Usul and R. Tolum, Int. J. Min. Process. **1**, 135 (1974).

[7] R. Woods, *A. M. Gaudin Memorial Volume*, edited by M. C. Fuerstenau (AIME, New York, 1976), p. 298.

[8] J. O. Leppinen, C. I. Basilio, and R. H. Yoon, Int. J. Min. Process. **26**, 259 (1989).

[9] C. C. Sui, S. H. R. Brienne, Z. H. Xu, and J. A. Finch, Int. J. Min. Process. **49**, 207 (1997).

[10] D. R. Nagaraj and J. S. Brinen, Int. J. Min. Process. **63**, 45 (2001).

[11] I. Persson, J. Coord. Chem. **32**, 261 (1994).

[12] M. C. Fuerstenau, U.S. Bureau of Mines Ino. Circ. **8818**, 7 (1980).
[13] A. Hung, I. Yarovsky, and S. P. Russo, Philos. Mag. Lett. (submitted).
[14] J. M. Guevremont, D. R. Strongin, and M. A. A. Schoonen, Surf. Sci. **391**, 109 (1997).
[15] K. M. Rosso, U. Becker, and M. F. Hochella, Am. Mineral. **85**, 2000 (2000).
[16] K. M. Rosso, U. Becker, and M. F. Hochella, Am. Mineral. **84**, 1999 (1999).
[17] A. Hung, J. Muscat, I. Yarovsky, and S. P. Russo, Surf. Sci. **513**, 511 (2002).
[18] A. Hung, J. Muscat, I. Yarovsky, and S. P. Russo, Surf. Sci. **520**, 111 (2002).
[19] Y. Numata, K. Takahashi, R. Liang, and T. Wakamatsu, Int. J. Min. Process. **53**, 75 (1998).
[20] J. A. Tossell and D. J. Vaughan, J. Colloid Interface Sci. **155**, 98 (1993).
[21] A. D. Becke, Phys. Rev. A **38**, 3098 (1988).
[22] J. P. Perdew and Y. Wang, Phys. Rev. B **45**, 13244 (1992).
[23] G. Kresse and J. Hafner, Phys. Rev. B **47**, 558 (1993); **49**, 14251 (1994).
[24] G. Kresse and J. Furthmuller, Comput. Mater. Sci. **6**, 15 (1996).
[25] G. Kresse and J. Furthmuller, Phys. Rev. B **54**, 11169 (1996).
[26] D. Vanderbilt, Phys. Rev. B **41**, 7892 (1990).
[27] J. D. Pack and H. J. Monkhorst, Phys. Rev. B **16**, 1748 (1977).
[28] *DMOL 96.0 Quantum Chemistry User Guide* (Molecular Simulations, San Diego, 1996).
[29] *Insight II 4.0.0 Molecular Modeling System User Guide* (Molecular Simulations, San Diego, 1996).
[30] J. Baker, J. Comput. Chem. **13**, 240 (1992).
[31] R. S. Mulliken, J. Chem. Phys. **23**, 1833 (1955).
[32] G. Winter, Rev. Inorg. Chem. **2**, 253 (1980).